Spatiotemporal Near-Field Spin Microscopy in Patterned Magnetic Heterostructures

J. Levy,[1] V. Nikitin,[1] J. M. Kikkawa,[1] A. Cohen,[1] N. Samarth,[2] R. Garcia,[2] and D. D. Awschalom[1]
[1]*Department of Physics, University of California, Santa Barbara, California 93106*
[2]*Department of Physics, The Pennsylvania State University, University Park, Pennsylvania 16802*
(Received 28 June 1995)

Low temperature femtosecond-resolved near-field scanning optical microscopy is used to image excitonic spin behavior in locally disordered magnetic semiconductor heterostructures. A contrast between luminescence intensity and polarization profiles yields marked differences between carrier diffusion and spin transport over a spin-dependent energy landscape sharply defined by focused ion beam implantation. Space-time spectroscopies reveal a spin component to the exciton evolution in the presence of a magnetic field. Fundamental limitations on the measurement of circularly polarized luminescence in the near field are also demonstrated.

PACS numbers: 75.70.Kw, 42.81.Wg, 73.20.Dx, 78.47.+p

Interest in the spin degrees of freedom of mesoscopic electronic systems has fueled a need to find new methods of probing them. The effects of interfaces, disorder, and local magnetic interactions strongly influence the transfer of spin angular momentum in small geometries, yet many of the underlying physical mechanisms are poorly understood. In recent years, magnetic semiconductor quantum wells, with greatly enhanced Zeeman splittings arising from strong Kondo-like exchange between localized paramagnetic spins and delocalized electronic states, have provided model systems in which to explore the dynamics of electronic spin interactions in reduced dimensions [1]. Such quantum structures have proven especially amenable to direct experimental measurements of spin scattering events over the relevant femtosecond and picosecond time scales [2]. Direct information concerning the *spatial* behavior of spin dynamical events over the corresponding mesoscopic length scales would be invaluable in developing a complete picutre of electronic spin scattering in low-dimensional systems.

To this end, we have developed a femtosecond-resolved low-temperature near-field scanning optical microscope (NSOM) to monitor the spatiotemporal evolution of excitonic spins in magnetic semiconductor heterostructures which are laterally patterned with a focused beam of Ga^+ ions. Polarization-resolved photoluminescence (PL) images reveal a spin-dependent energy landscape due to locally depressed Zeeman splittings in the implanted regions. Marked differences between carrier and spin behavior are observed through sharp contrasts in the intensity and polarization profiles, showing that excitonic diffusion has a minimal effect on the local magnetic interactions which contribute to Zeeman-split states. Time-resolved measurements suggest that the diffusion is driven by a spatially varying energy profile, and acquires a spin-dependent component in the presence of a magnetic field. Furthermore, a systematic study of the near- and far-field PL data demonstrates fundamental limitations on the measurement of polarization in the near-field regime.

The heterstructures consist of single 12 nm ZnSe/$Zn_{0.80}Cd_{0.20}Se$ molecular-beam-epitaxy–grown semiconductor quantum wells (QW) containing systematic distributions of magnetic ions (Mn^{2+}), and a nonmagnetic control structure [2]. Traditional magneto-optical studies of these structures show relatively narrow PL linewidths and large Zeeman splittings, making them ideal systems in which to study local spin-dependent interactions. To facilitate optical studies, the GaAs substrate is removed through polishing and etching to form a 300 μm diameter suspended circular film consisting of the $Zn_{0.80}Cd_{0.20}Se$ QW sandwiched between a ZnSe buffer (700 nm) and cap (100 nm) layers. A low-dosage ($10^4/\mu m^2$) 140 keV 100 nm diameter focused beam of Ga^+ ions is used to implant specific patterns in the etched structures.

Near-field PL experiments are performed with a compact NSOM which operates in a continuous He-gas flow optical cryostat at $T = 4$–300 K [3]. Subwavelength spatial resolution is achieved by using a piezoelectric transducer to scan the tip of a silver-coated tapered single-mode optical fiber close to the surface of interest [4], using shear-force feedback [5] to maintain a constant distance above the sample. The fiber aperture sizes are chosen to balance spatial resolution against photon shot noise, and are varied between 100 and 180 nm. Carriers are optically excited from the etched side and PL from the $n = 1$ heavy-hole excitonic peak collected with the fiber in the near field from the smooth opposite side of the structure. Circular polarization analysis and compensation of fiber birefringence are achieved with a variable wave plate and linear polarizer [3].

Figure 1(a) shows near-field low-temperature PL spectra [6] obtained from an intrinsic and nearby implanted region of the structure using a 100 nm fiber aperture positioned ~25 nm above the surface. The structures are excited with linearly polarized light from an Ar^+ ($E_{ex} = 2.707$ eV) or HeCd ($E_{ex} = 2.807$ eV) laser (~1 kW/cm^2) generating 500 excitons/μm^2 in steady state, and luminescence is collected in the Faraday configuration within fields $B = 0$–2 kG. In the intrinsic region, the magnetic

 0031-9007/96/76(11)/1948(4)$10.00

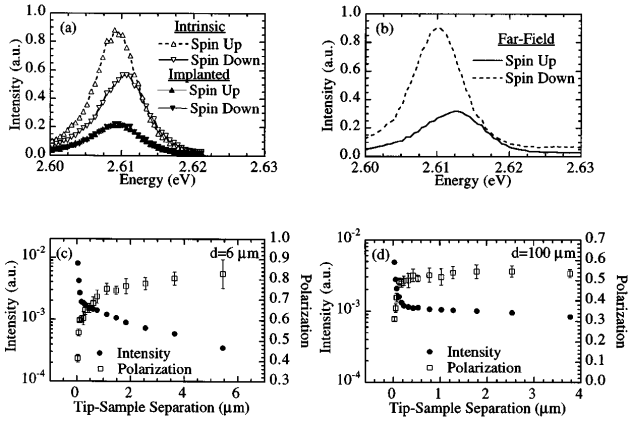

FIG. 1. (a) Near-field PL spectra for spin-up and spin-down excitons in an intrinsic and Ga^+ implanted region of a $ZnSe/Zn_{0.80}Cd_{0.20}Se$ quantum well containing 12 magnetic $\frac{1}{4}$ monolayer thick MnSe layers at $B = 2$ kG, $T = 5$ K, and excitation photon energy $E_{ex} = 2.807$ eV. (b) Far-field luminescence spectra of the same structure under otherwise identical conditions. (c) Near-field luminescence intensity and polarization measured from an unpatterned structure at $B = 2$ kG, $T = 5$ K as a function of tip-sample separation, exciting with a $d = 6$ μm laser spot size. (d) Same as (c), except $d = 100$ μm.

field causes the higher energy spin-up state to have a reduced amplitude compared to the energetically favored spin-down state, and an observed Zeeman splitting of 1.4 meV. Luminescence from a nearby implanted region exhibits smaller but equal intensities from both spin states which are now coincident in energy. This suggests that the structural disorder induced by the focused ion beam increases nonradiative decay channels and destroys the rotational symmetry of the lattice. The former decreases the quantum efficiency of the structure, while the latter reduces to zero the Zeeman splitting between the two spin states and hence the observed polarization.

Far-field measurements performed under otherwise identical conditions reveal a significantly larger Zeeman splitting of 2.7 meV [Fig. 1(b)]. We believe that the differences between Figs. 1(a) and 1(b) reflect fundamental limitations on the measurement and interpretation of polarized luminescence in the near-field regime. Figure 1(c) shows both luminescence intensity $I = I_+ + I_-$ and polarization $P \equiv (I_+ - I_-)/(I_+ + I_-)$, where $I_{+/-}$ is the intensity of left- or right-circularly polarized luminescence, measured at the PL peak $\lambda_{lum} = 475$ nm as a function of tip-sample separation z, with the excitation beam focused to a spot diameter $d = 6$ μm. As the tip approaches the surface from a distance $z \gg \lambda_{lum}$, the PL intensity increases moderately, then rises by a factor of 4, within the remaining 300 nm. A sharp knee in the intensity data clearly delineates the near- and far-field regimes. The PL polarization starts from a saturated value $P = 0.8$ for $z \gg d$, decreases slowly for $d > z > \lambda_{lum}$, then more rapidly for $z < \lambda_{lum}$, finally reaching the value $P = 0.4$ at the closest separation of 25 nm. We believe that the decrease in the observed polarization from its asymptotic value ($z \to \infty$) arises from two independent effects. (1) Because of the selection rules in a semiconductor, luminescence detected at an angle θ from the magnetic field axis will have a measured polarization $P(\theta) = P(0)\cos\theta$ [7]. The measured polarization is reduced when luminescence is collected over a large solid angle. Although the near-field tip collects light from all directions, its effective numerical aperture (NA) is determined by both d and z. The measured polarization

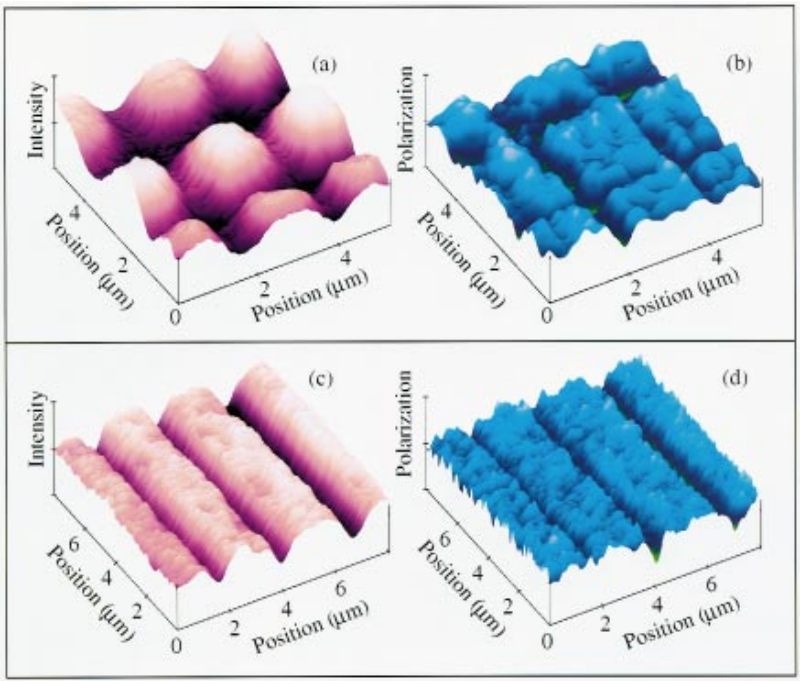

FIG. 2 (color). (a) NSOM luminescence intensity image for the Ga^+-implanted magnetic heterostructure of Fig. 1 ($T = 5$ K, $B = 2$ kG, $E_{ex} = 2.807$ eV). Pattern consists of alternating 300 and 600 nm stripes arranged both horizontally and vertically. (b) Polarization image over the same region. (c) Luminescence intensity for a second structure containing 24 magnetic $\frac{1}{8}$ monolayer thick MnSe layers implanted with 100, 200, and 400 nm thick vertical stripes left to right ($T = 5$ K, $B = 2$ kG, $E_{ex} = 2.707$ eV). (d) Polarization over the same region.

[Fig. 1(c)] increases with z as the NA is reduced, eventually reaching a saturated value of the far-field polarization. When the spot diameter is increased to $d \sim 100\ \mu$m [Fig. 1(d)], the numerical aperture is unaffected by changes in z over the same region, and thus the polarization is smaller and uniform. (2) At distances $z < \lambda_{\text{lum}}$, the sharp decrease in polarization is associated with coupling to the evanescent fields of the recombining excitons. Related effects have been observed in near-field studies of single molecules [8]. An intriguing explanation for the loss of polarization is that the evanescent fields do not propagate angular momentum and hence cannot couple to circularly polarized light in the far field.

NSOM images of the PL intensity and polarization are obtained by scanning the tip over the sample surface and collecting luminescence at a fixed detection energy. Figure 2(a) shows the PL intensity for one of the magnetic quantum well structures that has been subsequently patterned with alternating 300 and 600 nm horizontal and vertical stripes. The intensity is suppressed in the implanted regions, and recovers slowly in the intrinsic areas. In contrast, the measured polarization [Fig. 2(b)] is roughly constant in the intrinsic areas, and drops abruptly to zero as one moves into the implanted regions. The slow modulation of the intensity is attributed to exciton diffusion from intrinsic into nearby implanted regions. In contrast, the plateau of constant polarization over the intrinsic regions indicates that exciton diffusion does not affect the spin interactions which give rise to the large Zeeman shifts. Moreover, these results confirm that the ion-induced lattice damage is confined to the patterned areas. Figures 2(c) and 2(d) show similar results on a second quantum well structure with a different distribution of magnetic ions, patterned with vertical stripes of width 100, 200, 400, and 800 nm (not shown). In this case, the PL intensity profiles appear less rounded in the intrinsic regions compared to the cross-patterned image of Fig. 2(a), due to the one-dimensional patterning scheme in which exciton diffusion parallel to the implanted lines does not result in a loss of luminescence intensity. From the sharpness of the interfaces in Fig. 2(d) we estimate the NSOM resolution for these images to be $\sim$125 nm.

Spectrally resolved spatial scans provide a quantitative measure of the energy landscape for the two excitonic spin states. The PL and polarization extracted at the peak energy $E = 2.610$ eV are shown versus position in Figs. 3(a) and 3(b), yielding results similar to linecuts through the data of Fig. 2. Figure 3(c) shows the PL peak energy for both spin states, revealing a spin-dependent energy profile and small ($<$1 meV) scan-to-scan reproducible micron-scale variations in intrinsic regions which are most likely due to alloy fluctuations [9]. Subtraction of the two curves yields the spatially resolved Zeeman splitting, shown in Fig. 3(d). Much like the polarization, the splitting remains constant in intrinsic regions, dropping only in the implanted areas and indicating reduced magnetic interactions in these regions. Fluctuations of the Zeeman splitting in intrinsic regions are less pronounced than for the individual spin states [Fig. 3(c)], indicating little variation in the local g factor [10].

Time-resolved measurements are performed using a frequency-doubled mode-locked Ti:sapphire laser producing 130 fs pulses at 76 MHz tuned to $E_{\text{ex}} = 2.774$ eV (3×10^5 photons/μm^2). A luminescence intensity autocorrelation (LIA) technique [11], in which an inherent nonlinear dependence of the PL intensity with incident power, traditionally attributed to exciton-exciton scattering [12,13], is exploited to obtain time-resolved information about the lifetime of radiative excitonic states. The structure is excited by two equal-intensity linearly polarized pulses, separated by a variable time delay. Optical choppers modulate the two excitation beams at different frequencies, and phase-sensitive detection at the sum frequency probes the nonlinearities which arise from the

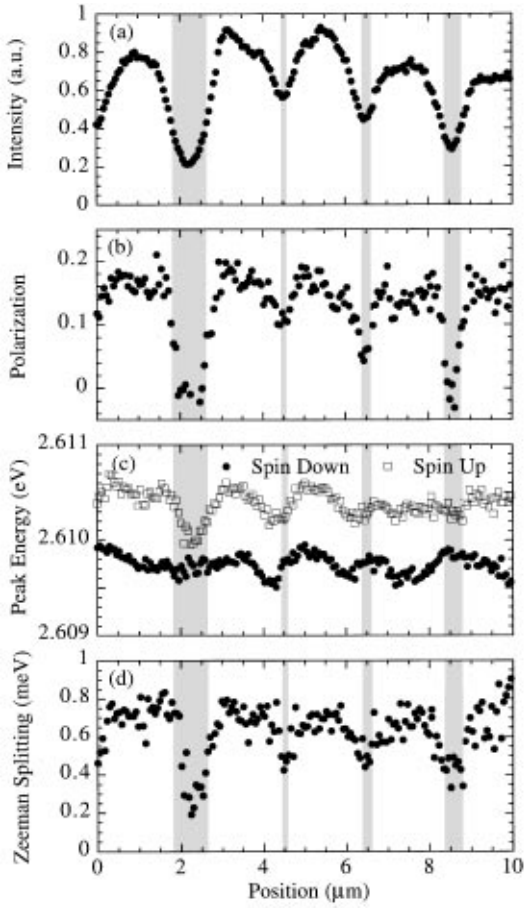

FIG. 3. (a) Luminescence intensity at $E = 2.610$ eV for the structure of Figs. 2(c) and 2(d) ($T = 5$ K, $B = 2$ kG, $E_{\text{ex}} = 2.707$ eV), extracted from a 2D scan of energy and position. Shaded regions depict the enginerred regions of ion implantation. (b) Polarization of luminescence at $E = 2.610$ eV. (c) Spatially resolved luminescence peak energies for spin-up and spin-down excitonic states. (d) Spatially resolved Zeeman splitting [difference of the two curves in (c)].

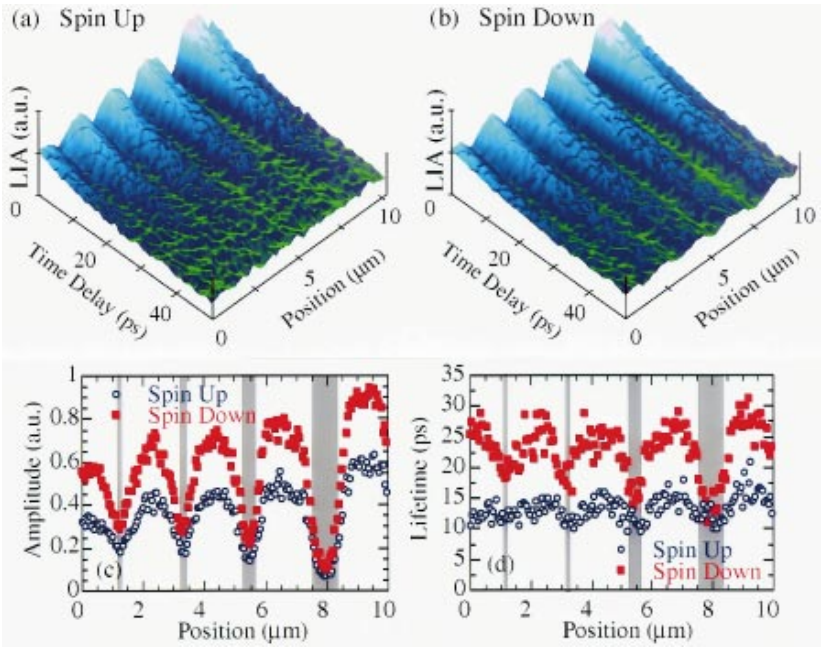

FIG. 4 (color). (a) Spatiotemporally resolved luminescence intensity autocorrelation (LIA) for spin-up excitonic state for the structure shown in Figs. 2(c) and 2(d) ($T = 5$ K, $B = 2$ kG, $E_{ex} = 2.774$ eV). (b) Same as (a), but for the spin-down state. (c) Single-exponential fit amplitude coefficients for both spin states. (d) Extracted lifetimes for both spin states.

temporal overlap of the two generated PL curves. The time decay of this signal is thus determined by the radiative recombination of the excitons and provides a measure of their lifetimes. The observed lifetimes in the intrinsic material agree with far-field time-resolved photoluminescence up-conversion measurements [2].

Figures 4(a) and 4(b) show the spatiallly resolved LIA for the stripe-patterned structure of Figs. 2(c) and 2(d) at $T = 5$ K and $B = 2$ kG for both spin-up and spin-down excitons, respectively. Our striking difference between the two images is in the lifetime, which is nearly twice as small for the spin-up state compared to the spin-down in the intrinsic region. A more quantitative comparison of the temporal decay of the recombining excitons is made by examining single-exponential fits to the data using the form $A\exp(-t/\tau)$, shown in Figs. 4(c) and 4(d). The amplitude (A) reduction for both spin states in the implanted regions [Fig. 4(c)] is more pronounced than the profiles shown in Fig. 2(a), due to the quadratic dependence of the LIA signal on luminescence intensity. The lifetime (τ) is reduced for both spin states in implanted regions, but the changes are much more pronounced for the spin-down state. These differences are attributed to an enhanced diffusion of spin-up excitons from the intrinsic to the nearby implanted regions, driven by the spin-dependent potentials seen in Fig. 3(c). An estimate of the diffusion constant D based on the profiles in Figs. 2 and 3 and the exciton lifetime yields $D = 0.2\,\mathrm{cm}^2/\mathrm{s}$, which is smaller than for III-V compounds [11,12] but reasonable given the larger inhomogeneous linewidth ~ 6 meV in these II-VI structures. As the width of the interface is decreased, the lifetime modulations for the spin-down state diminish, and eventually vanish for the spin-up state. Similar measurements taken at $T = 9$ K yield comparable lifetimes and reduced spin-dependent effects due to the decreased magnetization of the paramagnetic Mn spins [1]. In zero magnetic field, the two spin states are degenerate, and no spin-dependent effects are observed. Similar behavior is seen in the nonmagnetic control sample.

This work was supported by Grants ONR N00014-94-1-0297 and -0225, NSF DMR 92-07567, the NSF Center for Quantized Electronic Structures DMR 91-20007, AFOSR F49620-93-1-0446, and Digital Instruments, Inc.

[1] D. D. Awschalom and N. Samarth, in *Optics of Semiconductor Nanostructures*, edited by F. Hennenberger and S. Schmitt-Rink (Akademie Verlag, Berlin, 1993), and references therein; J. J. Baumberg *et al.*, Phys. Rev. B **50**, 7689 (1994).
[2] S. A. Crooker *et al.*, Phys. Rev. Lett. **75**, 505 (1995).
[3] J. Levy *et al.*, J. Appl. Phys. (to be published).
[4] E. Betzig *et al.*, Science **251**, 1468 (1991).
[5] E. Betzig, P. L. Finn, and J. S. Weiner, Appl. Phys. Lett. **60**, 2484 (1992).
[6] R. D. Grober *et al.*, Appl. Phys. Lett. **64**, 1421–1423 (1994).
[7] M. I. Dyakonov and V. I. Perel, in *Optical Orientaiton: Modern Problems in Condensed Matter Sciences*, edited by F. Meier and B. P. Zakharchenia (North-Holland, Amsterdam, 1984), Vol. 8, p. 27.
[8] W. P. Ambrose, P. M. Goodwin, J. C. Martin, and R. A. Keller, Phys. Rev. Lett. **72**, 160 (1994); W. E. Moerner, T. Plakhotnik, T. Irngartinger, and U. P. Wild, Phys. Rev. Lett. **73**, 2764 (1994).
[9] H. F. Hess *et al.*, Science **264**, 1740–1745 (1994).
[10] This result is not particularly surprising, since far-field measurements do not show any field dependence to the PL linewidth (see Ref. [2]).
[11] A. Olsson *et al.*, Appl. Phys. Lett. **41**, 659 (1982).
[12] D. Oberhauser *et al.*, Phys. Rev. B **47**, 6827 (1993).
[13] P. R. Newbury, K. Shahzad, and D. A. Cammack, Appl. Phys. Lett. **58**, 1065 (1991).